CrystEngComm

PAPER

View Article Online
View Journal | View Issue

Cite this: *CrystEngComm*, 2025, **27**, 5983

Compressing arsenic···halogen secondary bonds: a high-pressure structural study of arsenic(III) oxide intercalates with ammonium halides

Piotr A. Guńka, *[a] Sofija Milos, [b] Martin Ende, [c] Frederico Alabarse, [d] Ronald Miletich [b] and Kamil F. Dziubek [b]

Crystal structures of arsenic(III) oxide intercalation compounds with ammonium chloride ($NH_4Cl{\cdot}As_2O_3{\cdot}^1/_2H_2O$), ammonium bromide ($NH_4Br{\cdot}2As_2O_3$), and ammonium iodide ($NH_4I{\cdot}2As_2O_3$) have been determined under high pressure up to 12, 15 and 11 GPa, respectively. No phase transitions have been observed for the investigated compounds. The compression of arsenic···halogen secondary bonds, expressed as penetration indices of the bonds, has been shown to be a linear function of unit-cell volume ratio V/V_0, where V_0 is the unit-cell volume at ambient pressure, with similar slopes as the compression of arsenic···oxygen secondary bonds. The behavior of the arsenic coordination number, expressed as a first-order valence entropy coordination number, at high pressures and the stereoactivity of arsenic lone electron pairs in the studied intercalates are the same as in arsenic(III) oxide polymorphs – the former decreases linearly with V/V_0, while the latter remains unchanged. The high-pressure study lends further support to the fact that the nature of arsenic···halogen and arsenic···oxygen secondary bonds is the same.

Received 9th June 2025,
Accepted 28th July 2025

DOI: 10.1039/d5ce00593k

rsc.li/crystengcomm

Introduction

Intercalation compounds result from reversible inclusion, without covalent bonding, of one kind of molecule or ion in a solid matrix of another compound with a layered structure.[1] They are widely used, for instance, as electrode materials in batteries or catalysts. Some chalcogenide intercalates exhibit superconducting properties.[2,3] Arsenic(III) oxide intercalates are layered compounds, in which electroneutral layers of As_2O_3 separate sheets of cations and anions. The introduction of ions into the structure changes the conformation of individual As_2O_3 layers compared to arsenic(III) oxide polymorphs, but the connectivity of atoms within layers remains the same, and there are no covalent bonds between the ions and As_2O_3 layers. It has recently been reported that intercalates $CsBr{\cdot}2As_2O_3$ and $CsBr{\cdot}As_2O_3$ exhibit very high birefringence. The latter intercalate crystallizes in the polar space group $P6_3mc$ and has a very strong second harmonic generation response that is 20.5 times stronger than that of KH_2PO_4.[4]

Most of the known As_2O_3 intercalates, with the exception of the intercalate with NaBr, are hexagonal and comprise non-corrugated polar As_2O_3 layers that exhibit symmetry of layer group $P6mm$ and separate alternating flat layers of cations and anions (structure type **P**, see Fig. 1).[5,6] Anions

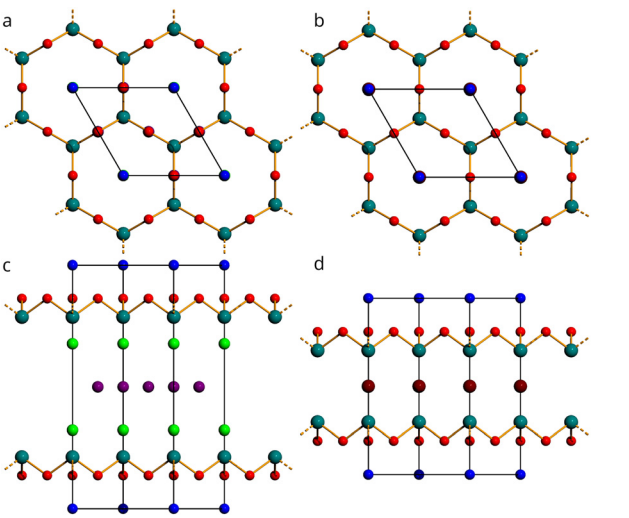

Fig. 1 Crystal structures of intercalates $NH_4Cl{\cdot}As_2O_3{\cdot}^1/_2H_2O$ (a and c) and $NH_4Br{\cdot}2As_2O_3$ (b and d). Views along the crystallographic [001] (a and b) and [120] (c and d) directions. As, O, N, Cl, and Br atoms are depicted as teal, red, blue, light green and brown spheres, respectively. Violet spheres denote N and O atoms of disordered ammonium cations and water molecules. H atoms are omitted for clarity.

[a] *Faculty of Chemistry, Warsaw University of Technology, ul. Noakowskiego 3, 00-664 Warszawa, Poland. E-mail: piotr.gunka@pw.edu.pl*
[b] *Institut für Mineralogie und Kristallographie, Universität Wien, Josef-Holaubek-Platz 2, A-1090 Wien, Austria*
[c] *Institute for Geosciences and Geography, Martin-Luther-University Halle-Wittenberg, 06120 Halle (Saale), Germany*
[d] *XPRESS Beamline, Elettra Sincrotrone Trieste S.C.p.A, AREA Science Park, I-34149 Basovizza, Trieste, Italy*

interact with arsenic(III) lone electron pairs (LEPs) forming the so-called secondary bonds, which are located *trans* with respect to the primary As–O bonds.[5] Cations template the As_2O_3 layers and are coordinated by oxygen atoms from the layers.[7] In the case of KCl and RbCl, hexagonal hydrated intercalates, $\mathbf{Y_{KCl}}$ and $\mathbf{Y'_{RbCl}}$, have been obtained in addition to anhydrous ones.[8,9] Meanwhile, for NH_4Cl, only a hydrated intercalate could be obtained so far.[10,11] In this compound, there is an additional layer containing disordered water molecules and ammonium cations. It is sandwiched between two layers of chloride anions (see Fig. 1).[11]

The aim of this work is to compare the compressibility and structural changes in the hydrated intercalate $NH_4Cl{\cdot}As_2O_3{\cdot}{}^1/_2H_2O$ ($\mathbf{Y_{NH_4Cl}}$) and in anhydrous ones $NH_4Br{\cdot}2As_2O_3$ ($\mathbf{P_{NH_4Br}}$) and $NH_4I{\cdot}2As_2O_3$ ($\mathbf{P_{NH_4I}}$). Another goal is to compare the pressure evolution of the As···halogen secondary bonds with the pressure dependence of As···O secondary bonds present in the As_2O_3 polymorphs.

Experimental and methodological details

High-pressure single-crystal X-ray diffraction

Single crystals of intercalates $\mathbf{Y_{NH_4Cl}}$, $\mathbf{P_{NH_4Br}}$ and $\mathbf{P_{NH_4I}}$ were obtained as described previously.[11] ETH-type diamond anvil cells (DACs) were used with pre-indented stainless steel gaskets with a thickness of *ca.* 120 μm. Diamond culets of 450 μm were used, and 200 μm holes were electrodrilled in the gaskets. Good-quality single crystals of the intercalates with typical dimensions of 80 μm × 60 μm × 15 μm were placed in the gasket holes together with ruby chips used for pressure determination.[12] Subsequently, DACs were gas loaded with argon used as a pressure transmitting medium (PTM). Diffraction data were collected at the Xpress beamline of the Elettra Synchrotron Radiation Facility using 0.4957 Å incident wavelength, 80 μm beam diameter and a PILATUS3 S 6M detector (from DECTRIS).[13] Raw frames were imported into CrysAlis^{PRO}, which was used for data reduction.[14] Crystal structures were refined using SHELXL 2019/3 invoked from Olex2 ver. 1.5 program.[15,16] Crystal structure models were analyzed using PLATON.[17] 3rd order Birch–Murnaghan (BM) equation of state (EoS) was fitted to the experimental $p(V)$ points using the EosFit software.[18,19] All unit-cell parameters are given in Tables S1–S3.

Valence entropy coordination number, bond-valence vector, and penetration index calculations

Bond valences (BVs) s_i were calculated according to the following equation: $s_i = \exp((R_0 - d_i)/B)$, where d_i, R_0 and B stand for the bond length of bond i, bond length of a bond with a valence of 1 and bond softness parameter, respectively.[20] Parameters determined by Gagné and Hawthorne were used for As–O bonds, by Brese and O'Keeffe for As···Cl interactions and by Brown for As···Br and As···I secondary bonds.[21–23] The dependence of R_0 on pressure was described using the relationship proposed by Brown.[24] The magnitude of bond-valence vectors $\boldsymbol{\nu}_i$ (BVVs) was calculated using the relationship derived by Zachara: $\|\boldsymbol{\nu}_i\| = s_i(1 - s_i/Q)$ where Q is the electric charge of the coordination center atomic core.[25] Zachara's BVV definition assumes that it is an integral of the electric field across a surface corresponding to a particular bond irrespective of the direction of that surface. Consequently, BVVs are aligned along the bonds they correspond to; the sum of BVVs around an unstrained coordination center is a zero vector. When a coordination center is electronically strained due to the presence of a stereoactive LEP, the resultant BVV can be brought back to zero by treating the LEP as a pseudoligand with $s_{LEP} \leq 2$. The equality holds for a fully stereoactive LEP and values smaller than two indicate partially stereoactive LEPs. When calculating BVVs, arsenic was treated as having a +5 oxidation state, so that the LEP could be treated as a pseudoligand. As no BV parameters for As(V)···Br and As(V)···I interactions are available, parameters for As(III) were used for these. This is justified by the fact that the difference between BV parameters for As(III)···Cl and As(V)···Cl interactions is small *i.e.* R_0 values differ by 0.02 Å and B is the same.

The strength of secondary interactions was also gauged using the penetration index defined as: $p_{AB} = 100{\cdot}(\nu_A + \nu_B - d_{AB})/(\nu_A + \nu_B - r_A - r_B)$, where ν_i and r_i stand for van der Waals and covalent radii of element i, while p_{AB} represents the penetration index of an interaction with distance d_{AB} between atoms A and B.[26] Covalent and van der Waals radii provided by Echeverria and Alvarez were utilized.[26]

The first-order valence entropy coordination number (^{1}VECN) was applied to quantitatively measure the coordination number of arsenic atoms forming both primary and secondary bonds. It was calculated according to the following formula: $\exp\left(-\sum_{i=1}^{N}(s_i/S)\ln(s_i/S)\right)$ where N is the number of bonds considered and $S = \sum_{i=1}^{N} s_i$. More details on the calculation of the ^{1}VECN are given elsewhere.[27]

Density functional theory (DFT) computations

Equation of state (EoS) modelling by DFT computations was only carried out for the intercalates $\mathbf{P_{NH_4Br}}$ and $\mathbf{P_{NH_4I}}$. The intercalate $\mathbf{Y_{NH_4Cl}}$ was not modelled computationally because there is additional positional disorder in that structure within the layer at $z = {}^1/_2$. Computations were carried out in a plane-wave basis set using Vienna *ab initio* simulation package VASP 6.4.2.[28] An energy cut-off of 1200 eV was applied with automatic generation of the Monkhorst–Pack net for sampling the first Brillouin zone, and the parameter value defining spacing between the points was set to 40.[29] PAW PBE potentials were applied.[30] Grimme's D3 correction for dispersion was used together with the Becke–Johnson damping function.[31,32] Geometry optimizations were stopped when the energy and maximum force per atom between steps

were smaller than 10^{-7} eV and 0.005 eV Å^{-1}, respectively. Two structural optimizations with only the unit-cell volume frozen followed by the final optimization with only atomic positions allowed to vary were carried out. Ammonium cations located at 0, 0, 0 are disordered and, for the purpose of modelling, we only considered cations with one of N–H bonds aligned along the crystallographic [001] direction.

Results and discussion

Crystal structure evolution with pressure

The pressure dependence of unit-cell volumes of the studied intercalates is plotted in Fig. 2 and the parameters of the fitted 3rd order BM EoS are listed in Table 1. $\mathbf{Y_{NH_4Cl}}$, $\mathbf{P_{NH_4Br}}$ and $\mathbf{P_{NH_4I}}$ undergo smooth compression under high pressure at least up to 12, 15 and 11 GPa, respectively. Apparently, all the investigated crystal structures of intercalates are so robust that argon non-hydrostaticity is only manifested in the increased mosaicity of the studied single crystals (see Fig. S1). Also, the $V(p)$ dependence for intercalates $\mathbf{P_{NH_4Br}}$ and $\mathbf{P_{NH_4I}}$ is in very good agreement with DFT predictions computed using the PBE-D3(BJ) model.

All the studied intercalates exhibit virtually the same linear compressibility along the <100> crystallographic direction (see Table S4 for ambient-pressure values, linear moduli, and their pressure derivatives of lattice parameters of the studied intercalates and Fig. S2). Intercalates $\mathbf{P_{NH_4Br}}$ and $\mathbf{P_{NH_4I}}$ also exhibit very similar linear compressibility along the [001] direction which results in very similar bulk moduli for the two compounds.

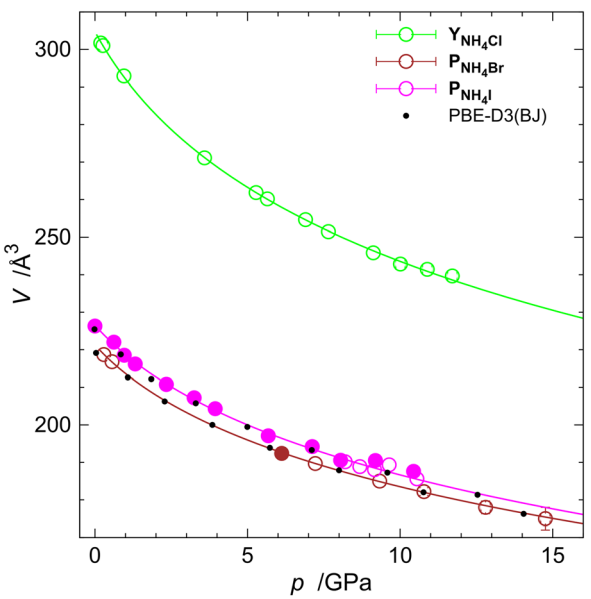

Fig. 2 Unit-cell volume of the studied intercalates plotted as a function of pressure. Open and closed circles correspond to pressure increase and decrease, respectively. Solid lines correspond to 3rd-order Birch–Murnaghan equations of states fitted to experimental data points, whereas black points correspond to the PBE-D3(BJ) DFT computations described thoroughly in the methodological details section.

Table 1 Parameters of the 3rd-order BM EoS fitted to the experimental and DFT data for the studied intercalates

	$\mathbf{Y_{NH_4Cl}}$	$\mathbf{P_{NH_4Br}}$		$\mathbf{P_{NH_4I}}$	
	Exp	Exp	DFT	Exp	DFT
V_0/Å^3	304.5(5)	221.3(7)	218.3(6)	226.5(7)	222.5(7)
B_0/GPa	21.3(11)	25(5)	35.2(14)	25(3)	34.1(15)
B_0'	6.8(5)	9(3)	5.8(2)	8(1)	5.82(19)

Pressure dependence of secondary As···halogen bonds

BVs as well as penetration indices of As···X secondary bonds are plotted as a function of pressure in Fig. 3. We have shown previously that the strength of As···X secondary bonds increases with the size and polarizability of the halide anion.[5] Here, the trend is clear for the intercalates $\mathbf{P_{NH_4Br}}$ and $\mathbf{P_{NH_4I}}$, while the intercalate $\mathbf{Y_{NH_4Cl}}$ seems to depart from it at first sight. However, we propose that high values of the As···Cl penetration index and BVs result from the different structures of this intercalate. The $s_{As\cdots Cl}$ BV values are 0.025, 0.026 and 0.024 v.u. for $\mathbf{P_{KCl}}$, $\mathbf{P_{RbCl}}$ and $\mathbf{P_{CsCl}}$, respectively and 0.041, 0.041 and 0.042 for $\mathbf{Y_{NH_4Cl}}$, $\mathbf{Y_{KCl}}$ and $\mathbf{Y'_{RbCl}}$, respectively.[33] Similarly, the penetration indices for $\mathbf{P_{MCl}}$

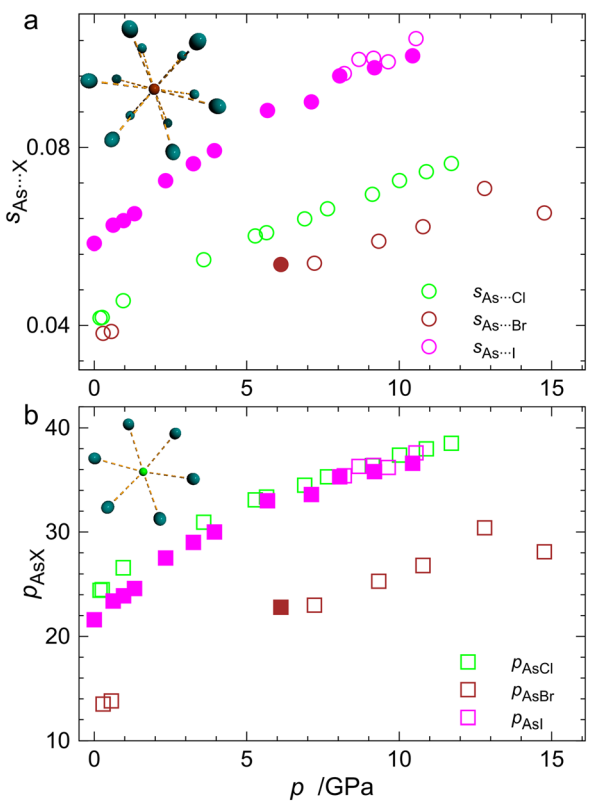

Fig. 3 As···X bond valences (a) and penetration indices (b) plotted as a function of pressure for the studied intercalation compounds. Insets present Br^- (a) and Cl^- (b) anions interacting with twelve As atoms in $\mathbf{P_{NH_4Br}}$ and six As atoms $\mathbf{Y_{NH_4Cl}}$, respectively.

range from 11.0% to 12.7% whereas for $\mathbf{Y_{MCl}}$ and $\mathbf{Y'_{RbCl}}$ from 23.9% to 24.6%. Thus, As⋯Cl interactions in $\mathbf{Y_{MCl}}$ are stronger than those in $\mathbf{P_{MCl}}$ and comparable to As⋯I secondary bonds in $\mathbf{P_{NH_4I}}$. This is likely the result of differences between crystal structures of intercalates $\mathbf{P_{MX}}$, where M stands for alkali metal and ammonium cations, and X for halide anions, and compounds $\mathbf{Y_{MCl}}$ as well as very similar $\mathbf{Y'_{RbCl}}$. Halide anions are involved in twelve As⋯X interactions in the former ones, while chloride anions only form six As⋯Cl secondary bonds in the latter compounds.

Penetration indices were chosen to compare the pressure evolution of As⋯X and As⋯O secondary bonds. They are plotted as a function of volume ratio V/V_0, where V_0 and V are the ambient pressure unit-cell volume and unit-cell volume at a given pressure, for the studied intercalates, as well as arsenic(III) oxide polymorphs, in Fig. 4. The ratio V/V_0 was chosen as a free variable instead of pressure to account for different compressibility, or bulk moduli, of the crystal structures where secondary bonding is present. Such a choice of the coordinate system led to the observation of linear correlations between penetration indices and volume ratios. Again, the slopes of the linear correlations for the intercalates $\mathbf{P_{NH_4Br}}$ and $\mathbf{P_{NH_4I}}$ are equal within two standard uncertainties (−81(5) and −89.8(14), respectively) while the slope of −69.3(14) for intercalate $\mathbf{Y_{NH_4Cl}}$ is slightly smaller in terms of absolute values, reflecting the fact that As⋯Cl secondary bond strengthening with pressure increase is less pronounced in $\mathbf{Y_{NH_4Cl}}$ intercalates than the strengthening of secondary bonding in $\mathbf{P_{NH_4X}}$ intercalates. The analogous slope for the As⋯O secondary bonds in arsenolite is −114.1(5).

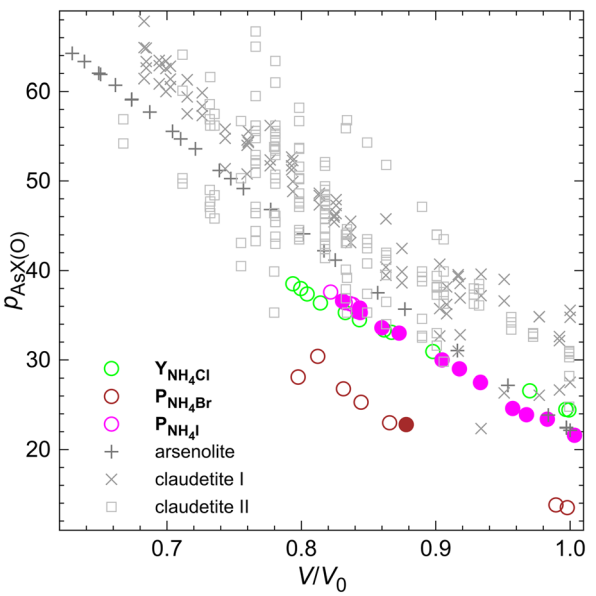

Fig. 4 Penetration indices of As⋯X and As⋯O secondary bonds in the studied intercalates and As_2O_3 polymorphs plotted as a function of V/V_0 unit-cell volume ratio. Data for arsenic(III) oxide polymorphs are taken from ref. 34–36.

Evolution of the arsenic coordination number and LEP stereoactivity with pressure

The first-order valence entropy coordination number of arsenic ($^1VECN_{As}$) and arsenic LEP stereoactivity expressed as the magnitude of the resultant BVV vector on arsenic atoms are plotted in Fig. 5 as a function of the V/V_0 ratio. The values of $^1VECN_{As}$ for the studied intercalates change with the unit-cell volume ratio in a very similar manner to those of As_2O_3 polymorphs, and the observed changes are linear. $^1VECN_{As}$ for the intercalates $\mathbf{P_{NH_4Br}}$ and $\mathbf{Y_{NH_4Cl}}$ are almost the same even though the As⋯Cl secondary bonds are weaker than the As⋯Br secondary bonds.[5] The reason for this is the same as in the case of penetration indices, namely the differences in crystal structures of the two types of intercalates. It is very likely, in our opinion, that chlorides tend to form the hydrated intercalates because the anions are relatively hard and are more keen on forming hydrogen bonds with water molecules than interactions with relatively soft LEPs of arsenic atoms. In the case of the softer bromide and iodide anions, no hydrated intercalates have been obtained so far as these anions are softer and form readily secondary interactions with arsenic LEPs.

The stereoactivity of arsenic LEPs in the studied intercalates does not change with pressure, like for arsenic(III) oxide, which indicates that pressure is an independent factor from LEPs causing strain in the coordination sphere of arsenic.[27] For a given pressure, the LEP stereoactivity

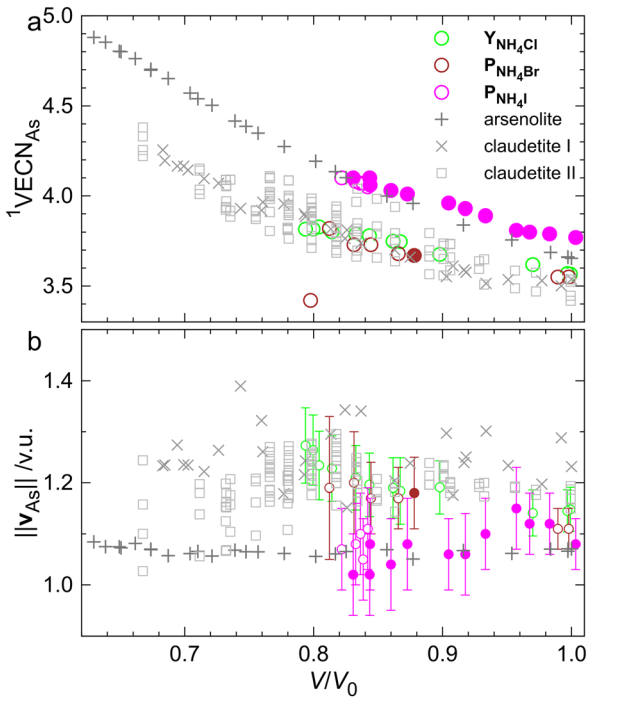

Fig. 5 First-order valence entropy coordination numbers of arsenic (a) and the magnitude of net BVV for arsenic (b) plotted as a function of the volume ratio V/V_0 for the studied intercalates and for arsenic(III) oxide polymorphs. Data for arsenic(III) oxide polymorphs are taken from ref. 34–36.

decreases slightly in the series $\mathbf{Y}_{NH_4Cl} > \mathbf{P}_{NH_4Br} > \mathbf{P}_{NH_4I}$ which also testifies to the fact that secondary bond strength increases in the same order *i.e.* As⋯Cl < As⋯Br < As⋯I.

The correlation of the first-order valence entropy coordination number of arsenic with the magnitude of the resultant BVV vector on arsenic atoms for the studied intercalates, arsenic(III) oxide polymorphs under HP, and arsenic(III) oxycompounds deposited in the Inorganic Crystal Structure Database is plotted in Fig. 6. The grey markers corresponding to ambient-pressure structures follow a general correlation that LEP stereoactivity, quantified by the magnitude of arsenic BVV, decreases with increasing pressure. The points corresponding to the HP structures of the studied intercalates depart from the correlation, similarly to the HP structures of As_2O_3 polymorphs. While an increasing coordination number with increasing pressure is expected, the fact that LEP stereoactivity does not decrease at HP is surprising.[37] Importantly, the points corresponding to the ambient-pressure structure of $\mathbf{Y}_{NH_4Cl}$ and other hydrated intercalates $\mathbf{Y}_{KCl}$ and $\mathbf{Y}'_{RbCl}$, represented by pentagons in Fig. 6, are located in the vicinity of the points corresponding to $\mathbf{P}_{MBr}$ intercalates. This reinforces our suggestion that decreasing the number of Cl⋯As contacts in **Y** (and **Y**′) intercalates compensates for the fact that Cl^- anions are harder bases than Br^- anions and that As⋯Cl secondary bonds are of comparable strength to As⋯Br secondary bonds when chloride anions form six such bonds and bromide anions form twelve (see Fig. 3a with the insets and Fig. 6).

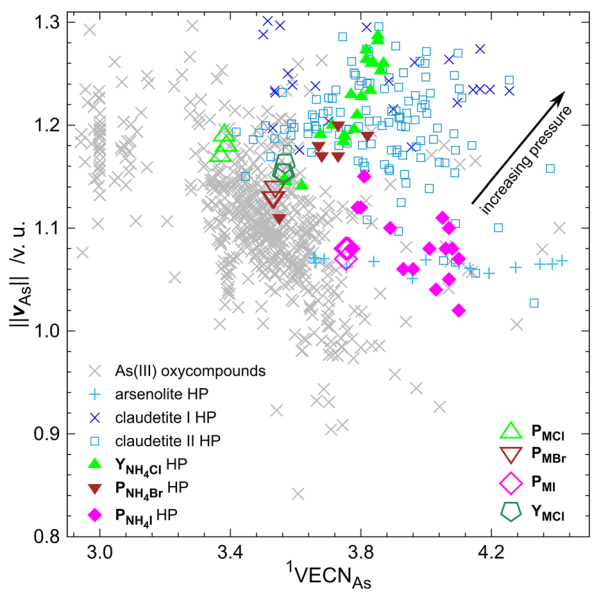

Fig. 6 The magnitude of net BVV for arsenic plotted as a function of the first-order valence entropy coordination number of arsenic for the studied intercalates, As_2O_3 polymorphs, and arsenic(III) oxycompounds deposited in the Inorganic Crystal Structure Database. HP in the legend denotes high-pressure structures. The larger markers indicated at the bottom right correspond to ambient-pressure structures of intercalates. The black arrow indicates the compression of the systems. Data for arsenic(III) oxide polymorphs, for arsenic(III) oxycompounds, and for intercalates are taken from ref. 5, 9, 27 and 34–36.

Conclusions

Crystal structures of three arsenic(III) oxide intercalates with ammonium halides have been determined under high pressure for the first time. They do not undergo any phase transitions up to the highest pressures reached in this study (12 GPa for $\mathbf{Y}_{NH_4Cl}$, 15 GPa for $\mathbf{P}_{NH_4Br}$ and 11 GPa for $\mathbf{P}_{NH_4I}$). Analysis of the pressure dependence of penetration indices of As⋯X secondary bonds, where X stands for a halogen, revealed that their dependence becomes linear when pressure is replaced by the unit-cell volume ratio V/V_0, where V_0 is the ambient pressure volume. This is caused by the fact that the V/V_0 ratio takes into account different compressibility, or bulk moduli, of the compared crystal structures. Not only the penetration indices but also the first-order valence entropy coordination number of arsenic decrease linearly with volume ratio V/V_0. Both these relationships are also linear for As⋯O secondary bonds present in arsenic(III) oxide polymorphs. The stereoactivity of arsenic LEPs is virtually unchanged upon pressure increase indicating that pressure increases the arsenic coordination number by making the crystal structures "more crowded" without decreasing the LEP stereoactivity similar to arsenic(III) oxide polymorphs. It will be very interesting to carry out an analogous study for a series of As_2O_3 intercalates with potassium halides, which includes anhydrous $\mathbf{P}_{KCl}$, $\mathbf{P}_{KBr}$, and $\mathbf{P}_{KI}$ and hydrated $\mathbf{Y}_{KCl}$. It should allow us to verify our suggestion that the increased strength of As⋯Cl secondary bonds in intercalate $\mathbf{Y}_{NH_4Cl}$ compared to the expectations from the trend of decreasing strength of secondary interactions As⋯I > As⋯Br > As⋯Cl is the result of a smaller number of secondary bonds formed by chloride anions in intercalate $\mathbf{Y}_{NH_4Cl}$ than in compounds $\mathbf{P}_{NH_4X}$.

Author contributions

P. A. G. – conceptualization, investigation, writing – original draft, writing – review & editing; S. M. – investigation, writing – review & editing; M. E. – investigation, writing – review & editing; F. A. – resources, methodology, writing – review & editing; R. M. – resources, writing – review & editing; K. F. D. – investigation, formal analysis, writing – review & editing.

Conflicts of interest

There are no conflicts to declare.

Data availability

Supplementary information available: figures with the studied crystals' mosaicities and unit cell parameters plotted as a function of pressure; a table with linear bulk moduli. See DOI: **https://doi.org/10.1039/D5CE00593K**.

CSD 2440780–2440816 contain the supplementary crystallographic data for this paper.

Raw diffraction data are available at Zenodo at **https://doi.org/10.5281/zenodo.15356607**.

Acknowledgements

This research has been funded by the Polish National Science Centre (project no. 2020/39/D/ST4/00128). Elettra Sincrotrone Trieste is gratefully acknowledged for providing beam time for the experiments at the Xpress beamline (Proposals 20230005 and 20240142). Fruitful discussions with Ross J. Angel and G. Diego Gatta are gratefully acknowledged.

Notes and references

1 T. I. U. of P. and A. Chemistry (IUPAC), IUPAC – intercalation compounds (I03076), **https://goldbook.iupac.org/terms/view/I03076**, (accessed May 22, 2024).
2 R. A. Klemm, *Phys. C*, 2015, **514**, 86–94.
3 A. Krzton-Maziopa, Z. Shermadini, E. Pomjakushina, V. Pomjakushin, M. Bendele, A. Amato, R. Khasanov, H. Luetkens and K. Conder, *J. Phys.: Condens. Matter*, 2011, **23**, 052203.
4 W. Zeng, Y. Tian, H. Zeng, Z. Lin and G. Zou, *Angew. Chem., Int. Ed.*, 2025, **64**, e202422818.
5 M. Dąbrowski, W. Wrześniewska, A. Prystupiuk, J. Zachara and P. A. Guńka, *Cryst. Growth Des.*, 2023, **23**, 6081–6085.
6 F. Pertlik, *J. Solid State Chem.*, 1987, **70**, 225–228.
7 P. A. Guńka, K. Kraszewski, Y.-S. Chen and J. Zachara, *Dalton Trans.*, 2014, **43**, 12776–12783.
8 M. A. Domański, K. Kraszewski, P. Paluch and P. A. Guńka, *Cryst. Growth Des.*, 2021, **21**, 5215–5222.
9 P. Michalak, P. Paluch and P. A. Guńka, *Cryst. Growth Des.*, 2022, **22**, 711–717.
10 M. Edstrand and G. Blomqvist, *Ark. Kemi*, 1955, **8**, 245–256.
11 W. Wrześniewska, P. Paluch and P. A. Guńka, *Acta Crystallogr., Sect. B: Struct. Sci., Cryst. Eng. Mater.*, 2023, **79**, 207–212.
12 A. Dewaele, M. Torrent, P. Loubeyre and M. Mezouar, *Phys. Rev. B: Condens. Matter Mater. Phys.*, 2008, **78**, 104102.
13 P. Lotti, S. Milani, M. Merlini, B. Joseph, F. Alabarse and A. Lausi, *J. Synchrotron Radiat.*, 2020, **27**, 222–229.
14 *CrysAlisPro Software system ver. 171.43 Rigaku Oxford Diffraction*, Oxford, UK, 2023.
15 G. M. Sheldrick, *Acta Crystallogr., Sect. C: Struct. Chem.*, 2015, **71**, 3–8.
16 O. V. Dolomanov, L. J. Bourhis, R. J. Gildea, J. A. K. Howard and H. Puschmann, *J. Appl. Crystallogr.*, 2009, **42**, 339–341.
17 A. L. Spek, *J. Appl. Crystallogr.*, 2003, **36**, 7–13.
18 F. Birch, *Phys. Rev.*, 1947, **71**, 809–824.
19 J. Gonzalez-Platas, M. Alvaro, F. Nestola and R. Angel, *J. Appl. Crystallogr.*, 2016, **49**, 1377–1382.
20 I. D. Brown, *The Chemical Bond in Inorganic Chemistry: The Bond Valence Model*, Oxford University Press, Oxford, 2016.
21 O. C. Gagné and F. C. Hawthorne, *Acta Crystallogr., Sect. B: Struct. Sci., Cryst. Eng. Mater.*, 2015, **71**, 562–578.
22 N. E. Brese and M. O'Keeffe, *Acta Crystallogr., Sect. B: Struct. Sci.*, 1991, **47**, 192–197.
23 I. D. Brown, Bond-valence parameters, **https://www.iucr.org/resources/data/datasets/bond-valence-parameters**, (accessed April 25, 2023).
24 I. D. Brown, P. Klages and A. Skowron, *Acta Crystallogr., Sect. B: Struct. Sci.*, 2003, **59**, 439–448.
25 J. Zachara, *Inorg. Chem.*, 2007, **46**, 9760–9767.
26 J. Echeverría and S. Alvarez, *Chem. Sci.*, 2023, **14**, 11647–11688.
27 P. A. Guńka and J. Zachara, *Acta Crystallogr., Sect. B: Struct. Sci., Cryst. Eng. Mater.*, 2019, **75**, 86–96.
28 G. Kresse and J. Furthmüller, *Phys. Rev. B: Condens. Matter Mater. Phys.*, 1996, **54**, 11169–11186.
29 H. J. Monkhorst and J. D. Pack, *Phys. Rev. B: Solid State*, 1976, **13**, 5188–5192.
30 G. Kresse and D. Joubert, *Phys. Rev. B: Condens. Matter Mater. Phys.*, 1999, **59**, 1758–1775.
31 S. Grimme, J. Antony, S. Ehrlich and H. Krieg, *J. Chem. Phys.*, 2010, **132**, 154104.
32 S. Grimme, S. Ehrlich and L. Goerigk, *J. Comput. Chem.*, 2011, **32**, 1456–1465.
33 Both **Y** and **Y′** intercalates are hydrated. The only difference between them lies in the structure of the disordered layer located at $z = {}^1/_2$.
34 P. A. Guńka, K. F. Dziubek, A. Gładysiak, M. Dranka, J. Piechota, M. Hanfland, A. Katrusiak and J. Zachara, *Cryst. Growth Des.*, 2015, **15**, 3740–3745.
35 P. A. Guńka, M. Dranka, M. Hanfland, K. F. Dziubek, A. Katrusiak and J. Zachara, *Cryst. Growth Des.*, 2015, **15**, 3950–3954.
36 P. A. Guńka, M. Hanfland, Y.-S. Chen and J. Zachara, *CrystEngComm*, 2021, **23**, 638–644.
37 W. Grochala, R. Hoffmann, J. Feng and N. W. Ashcroft, *Angew. Chem., Int. Ed.*, 2007, **46**, 3620–3642.

